POLITECNICO DI TORINO
Repository ISTITUZIONALE

Modeling of Josephson Traveling Wave Parametric Amplifiers

(Article begins on next page)

12 June 2023

12 June 2023

Modeling of Josephson Traveling Wave Parametric Amplifiers

C. Guarcello, G. Avallone C. Barone, M. Borghesi, S. Capelli, G. Carapella, A.P. Caricato, I. Carusotto, A. Cian, D. Di Gioacchino, E. Enrico, P. Falferi, L. Fasolo, M. Faverzani, E. Ferri, G. Filatrella, C. Gatti, A. Giachero, D. Giubertoni, V. Granata, A. Greco, D. Labranca, A. Leo, C. Ligi, G. Maccarrone, F. Mantegazzini, B. Margesin, G. Maruccio, C. Mauro, R. Mezzena, A.G. Monteduro, A. Nucciotti, L. Oberto, L. Origo, S. Pagano, V. Pierro, L. Piersanti, M. Rajteri, A. Rettaroli, S. Rizzato, A. Vinante, and M. Zannoni

Abstract—**The recent developments in quantum technologies, as well as advanced detection experiments, have raised the need to detect extremely weak signals in the microwave frequency spectrum. To this aim, the Josephson travelling wave parametric amplifier, a device capable of reaching the quantum noise limit while providing a wide bandwidth, has been proposed as a suitable cryogenic front-end amplifier. This work deals with the numerical study of a Josephson travelling wave parametric amplifier, without approximations regarding the nonlinearity of the key elements. In particular, we focus on the investigation of the system of coupled nonlinear differential equations representing all the cells of the Josephson travelling wave parametric amplifier, with proper input and output signals at the boundaries. The investigation of the output signals generated by the parametric amplification process explores the phase-space and the Fourier spectral analysis of the output voltage, as a function of the parameters describing the pump and signal tones that excite the device. Beside the expected behavior, i.e., the signal amplification, we show that, depending on the system operation, unwanted effects (such as pump tone harmonics, incommensurate frequency generation, and noise rise), which are not accounted for in simple linearized approaches, can be generated in the whole nonlinear system.**
1

C. Guarcello, G. Carapella, and V. Granata are with Physics Dept., University of Salerno, Fisciano (SA), Italy and with INFN - Gruppo Collegato Salerno, Fisciano (SA) 84084, Italy (e-mail: cguarcello@unisa.it; gcarapella@unisa.it; vgranata@unisa.it).

G. Avallone and C. Mauro are with INFN - Gruppo Collegato Salerno, 84084 Fisciano (SA), Italy (e-mail: guavallone@unisa.it; cmauro@na.infn.it).

C. Barone and S. Pagano are with Physics Dept., University of Salerno, Fisciano (SA), Italy, with INFN - Gruppo Collegato Salerno, Fisciano (SA) 84084, Italy and with CNR-SPIN Salerno section, 84084 Fisciano (SA), Italy (e-mail: cbarone@unisa.it; spagano@unisa.it).

M. Borghesi, S. Capelli, M. Faverzani, E. Ferri, A. Giachero, D. Labranca, A. Nucciotti, L. Origo, and M. Zannoni are with Physics Dept., University of Milano-Bicocca, 20126 Milano, Italy and with INFN - Sezione di Milano Bicocca, 20126 Milano, Italy (e-mail: matteo.borghesi@unimib.it; silvia.capelli@unimib.it; marco.faverzani@unimib.it; elena.ferri@unimib.it; andrea.giachero@unimib.it; danilo.labranca@mib.infn.it; angelo.nucciotti@unimib.it; luca.origo@mib.infn.it; mario.zannoni@mib.infn.it).

A.P. Caricato, A. Leo, G. Maruccio, A. Monteduro, and S. Rizzato are with Mathematics and Physics Dept., University of Salento, 73100 Lecce, Italy and with INFN – Sezione di Lecce, 73100 Lecce, Italy (e-mail: annapaola.caricato@unisalento.it; angelo.leo@unisalento.it; giuseppe.maruccio@unisalento.it; annagrazia.monteduro@unisalento.it; silvia.rizzato@unisalento.it).

I. Carusotto is with CNR INO, 38123 Povo (TN), Italy and with Physics Dept., University of Trento, 38123, Povo (TN), Italy (e-mail: iacopo.carusotto@ino.cnr.it).

A. Cian, D. Giubertoni, F. Mantegazzini, and B. Margesin are with Fondazione Bruno Kessler, 38123 Povo (TN), Italy and with INFN - TIFPA, 38123 Povo (TN), Italy (e-mail: acian@fbk.eu; giuberto@fbk.eu; fmantegazzini@fbk.eu; margesin@fbk.eu).

D. Di Gioacchino, C. Gatti, C. Ligi, G. Maccarrone, L. Piersanti, and A. Rettaroli are with INFN - Laboratori Nazionali di Frascati, 00044 Frascati (RM), Italy (e-mail: daniele.digioacchino@lnf.infn.it; claudio.gatti@lnf.infn.it; carlo.ligi@lnf.infn.it; giovanni.maccarrone@lnf.infn.it; luca.piersanti@lnf.infn.it; alessio.rettaroli@lnf.infn.it).

E. Enrico and L. Oberto are with INRiM - Istituto Nazionale di Ricerca Metrologica, 10135 Torino, Italy and with INFN - TIFPA, 38123 Povo (TN), Italy (e-mail: e.enrico@inrim.it; l.oberto@inrim.it).

P. Falferi and A. Vinante are with Fondazione Bruno Kessler, 38123 Povo (TN), Italy, with INFN - TIFPA, 38123 Povo (TN), Italy and with CNR IFN, 38123 Povo (TN), Italy (e-mail: paolo.falferi@unitn.it; andrea.vinante@ifn.cnr.it).

L. Fasolo and A. Greco are with INRiM - Istituto Nazionale di Ricerca Metrologica, 10135 Torino, Italy and with Politecnico di Torino, 10129 Torino, Italy (e-mail: luca_fasolo@polito.it; angelo.greco@polito.it).

G. Filatrella is with Science and Technology Dept., University of Sannio, 82100 Benevento, Italy and with INFN - Gruppo Collegato Salerno, 84084 Fisciano (SA), Italy (e-mail: filatr@unisannio.it).

R. Mezzena is with Physics Dept., University of Trento, 38123, Povo (TN), Italy and with INFN - TIFPA, 38123 Povo (TN), Italy (e-mail: renato.mezzena@unitn.it).

V. Pierro is with Engineering Dept., University of Sannio, 82100 Benevento, Italy and with INFN - Gruppo Collegato Salerno, 84084 Fisciano (SA), Italy (e-mail: pierro@unisannio.it).

M. Rajteri is with INRiM - Istituto Nazionale di Ricerca Metrologica, 10135 Torino, Italy and with INFN - Sezione di Torino, 10125 Torino, Italy (e-mail: m.rajteri@inrim.it).

Color versions of one or more of the figures in this paper are available online at http://ieeexplore.ieee.org.

Digital Object Identifier will be inserted here upon acceptance.

Index Terms—**Josephson junctions (JJs), Microwave amplifiers, Superconducting microwave devices, Parametric Amplifiers, Josephson Travelling Wave Parametric Amplifiers**

I. INTRODUCTION

Recently, quantum parametric amplifiers have attracted a lot of attention due to their versatility and relevance in concrete applications, especially in the field of superconductivity, ranging from quantum optics [1, 2], quantum measurement [3], qubit readout [4], and single photon microwave detection [5, 6, 7, 8, 9,10]. Often these applications require to read multiple detectors as well as to implement multiplexing strategy, so that large bandwidth amplifiers with low noise are needed. Quantum parametric amplifiers have the undoubted advantage of providing high gain and, at the same time, make it possible to approach, and even to overcome under nontrivial conditions [11], the quantum noise limit. The phenomenon of parametric amplification relies on a *frequency mixing* induced by circuit
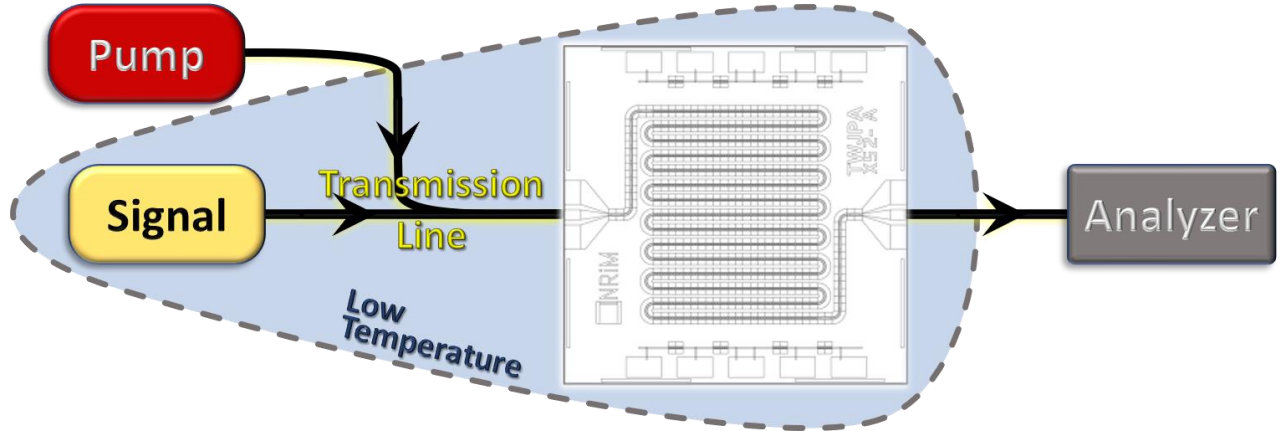
Fig. 1. Cartoon of the experimental setup, including the layout of a TWJPA Chip TWJPA_X52 (size 10x10 mm^2) based on a sequence of 990 elementary cells, each formed by an RF-SQUID in series and an interdigital capacitor to ground. The pump and signal input sources and the output analyzer are also indicated.

nonlinearity: in practice, a small signal can be amplified by coupling it with a larger pump tone, thanks to an energy transfer from the pump to the signal. The concrete implementation of these devices often revolves around Josephson systems that, thanks to their non-linear inductance, can work as a tunable non-linear resonator, in which the resonance frequency can be adjusted to achieve optimized amplification.

II. JOSEPHSON TRAVELLING WAVE PARAMETRIC AMPLIFIER DESIGN

Josephson parametric amplifiers (JPAs) transfer power from a strong pump tone to a weak signal thanks to the non-linearity of the Josephson tunnel junction and a frequency mixing process. For a comprehensive overview of recent developments on JPAs, refer to [12]. Although JPAs can reach the quantum noise level, they exhibit limited bandwidth, dynamic range, and linearity [12,13]. The narrow bandwidth of these devices limits their use "in series", for example for qubit readout (where the possibility to read a few qubits per amplifier is a limiting factor for scaling up quantum processors [14, 15]) or axion detection (where it is not possible to scale the experiment to a series of cavities [16, 17,18]).

In contrast, superconducting travelling wave parametric amplifiers (TWPAs) still offer limited quantum noise, but at the same time give a wide bandwidth. Although the theory to describe these amplifiers is quite dated [19,20], they are nowadays gaining more and more popularity and new proposals and realizations appear frequently. Superconducting TWPAs work on the parametric amplification of microwaves travelling along a transmission line which contains non-linear elements, often implemented by JJs; the dependence on the current of the Josephson inductance is responsible for the parametric mixing and amplification. By injecting a large-amplitude pump tone, at frequency v_{pump}, together with a weak signal to be amplified, at frequency v_{sign}, the current of the large amplitude pump tone modulates the non-linear Josephson inductance, thus coupling the pump to the signal and possibly producing the amplification of the latter, but also eventually inducing an idle tone at

frequency v_{idle}. According to the current dependence of the nonlinearity, two different operating regimes can be distinguished: a four-wave mixing (4WM), in which the pump frequency is half of the sum of the signal frequency and the idler signal, i.e., $2v_{pump} = v_{sign} + v_{idle}$, and a three-wave mixing (3WM), in which the pump frequency is just equal to this sum, i.e., $v_{pump} = v_{sign} + v_{idle}$, which emerges when biasing the system by current and/or magnetic field. These relations correspond to the conservation of energy of the photons participating in the mixing process.

In this work, we focus on modeling a specific kind of device, i.e., the Josephson TWPA (JTWPA), that is made by a series of SQUIDs [21, 22, 23, 24, 25, 26, 27, 28] and a capacitive shunt to ground. Usually, these devices provide almost quantum-limited noise and large bandwidth (about 6 GHz centered at 7 GHz), but the gain is typically limited (<20 dB) as well as the dynamic range (<−90 dBm). For a review on JTWPAs, see Refs. [29,30].

An example of an experimental setup, which will be used as base for models and simulations, is depicted in Fig. 1. Here, the core element is the first version of JTWPA realized at INRiM within DARTWARS project [31,32], whose basic cell is an rf-SQUID and a capacitor to ground. The figure sketches also the pump and signal tones injected to the JTWPA through a transmission line, and the analyzer receiving the output signal.

III. MODELING AND NUMERICAL SIMULATIONS

The details of the JTWPA modeled in this work are given in Fig. 2. The specific values assumed for the system parameters have been extracted from experimental measurements of the device in Ref. [32]. The gray shaded panel of Fig. 2 focuses the generic n^{th} cell of the JTWPA, while the top line contains the left and right boundary elements. In particular, the JTWPA considered in this work consists of a series of $N = 990$ identical
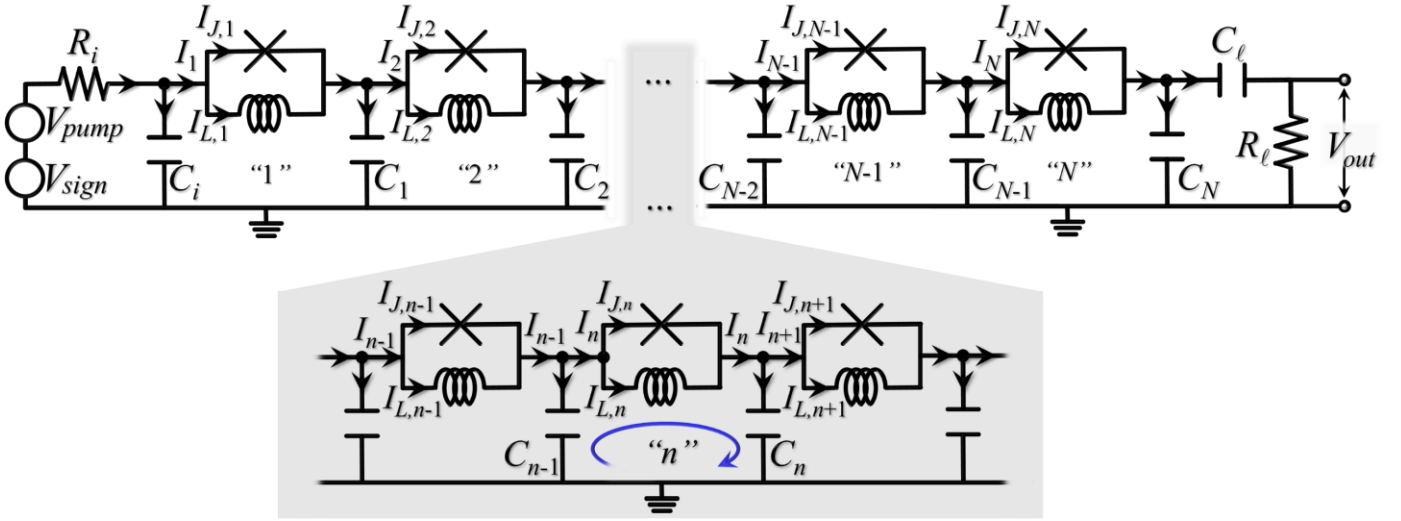
Fig. 2. Equivalent electrical circuit of a JTWPA. On the top: left and right cells, including the input pump and signal tones, V_{pump} and V_{sign}, respectively, the input and load resistances and capacitances, R_i, C_i, R_ℓ, C_ℓ. The output voltage is dropped across the load resistor. In the gray shaded box: detail of a generic cell composing the series of N = 990 elements forming the JTWPA.

cells, each including the rf-SQUID, formed by a JJ in parallel to a geometric inductance $L_{g,n} = 120$ pH, and a capacitor $C_{g,n} = 24$ fF. The first element of the chain includes the pump and signal voltage source, V_{pump} and V_{sign}, with the input resistance and capacitor $R_i = 50\ \Omega$ and $C_i = 24$ fF, respectively, while the last element has the load resistance and capacitor, $R_\ell = 50\ \Omega$ and $C_\ell = 1$ nF, respectively.

The equations for a generic nth cell are:

$$I_n - I_{n+1} = \dot{q}_n \tag{1}$$

$$I_n = I_{J,n} + I_{L,n} = I_{J,n} + \frac{\hbar}{2e}\frac{\varphi_n}{L_{g,n}} \tag{2}$$

$$\frac{\hbar}{2e}\frac{d\varphi_n}{dt} + \frac{q_n}{C_{g,n}} = \frac{q_{n-1}}{C_{g,n-1}} \tag{3}$$

The current $I_{J,n}$ through the junction is described within the Resistively and Capacitively Shunted Junction (RCSJ) model [33],

$$I_{J,n} = C_J \frac{\hbar}{2e}\frac{d^2\varphi_n}{dt^2} + \frac{1}{R_J}\frac{\hbar}{2e}\frac{d\varphi_n}{dt} + I_c \sin\varphi_n, \tag{4}$$

assuming a critical current $I_c = 2\ \mu$A, a quasiparticle resistance $R_J = 20$ kΩ, and a junction capacitance $C_J = 200$ fF. The R_J value has been chosen large enough not to influence the overall dynamics: it is much larger than the junction capacitive and reactive impedance in the range 1-20 GHz. The chosen values give a plasma frequency equal to $\nu_p \approx 27.7$ GHz. The Josephson current is assumed to be sinusoidally dependent on the phase difference, i.e., $I(\varphi) = I_c \sin\varphi$. Recalling the 2nd Josephson relation for the voltage, i.e., $V = \hbar/(2e)d\varphi/dt$, it is straightforward to obtain the current-voltage characteristic of a nonlinear inductor as:

$$V = \frac{\hbar/2e}{I_c\cos(\varphi)}\frac{dI}{dt} = L_{J0}(\varphi)\ \frac{dI}{dt} \tag{5}$$

with

$$L_{J0}(\varphi) = \frac{\hbar/2e}{I_c\cos(\varphi)} \tag{6}$$

being the Josephson inductance. In the case of non-null DC bias current I_b, the Josephson inductance becomes:

$$L_J(\varphi) = \frac{L_{J0}(\varphi)}{\sqrt{1-\left(\frac{I_b}{I_c}\right)^2}} \tag{7}$$

In other words, the bias current acts as a control knob for tuning the Josephson inductance, which becomes larger as I_b increases, up to diverge for $I_b \rightarrow I_c$.

Theoretical approaches [34,35] linearize the Josephson inductance, and consider a simplified scenario in the lower-order approximation. Instead, we propose to tackle the problem in its full complexity, solving the system of N coupled differential equations, see e.g. [26], including the proper boundary conditions that mimic the signal generators and the output transmission line. The dynamics is finally obtained by integrating the system of N coupled differential equation with a finite-difference method based on a tridiagonal algorithm; the time step and the integration time are set to $\Delta t = 0.01$ and $t_{max} = 10^4$, respectively. This approach makes it also possible, in principle, to model both the imperfections that affect practical realization of the device elements, which can certainly be not identical, and the effects induced by thermal noise. However, the cells forming the JTWPA are assumed identical in this work, while the effects produced by parameter value distributions and thermal noise will be the subject of a future work, e.g., see Ref. [36].

In the following sections we discuss first the case in which only the pump tone is injected into the system, i.e., $V_{sign} = 0$, in order to explore the input pump attenuation, and then we consider both the pump and the signal tones and we investigate the possibility to amplify the signal taking advantage of the
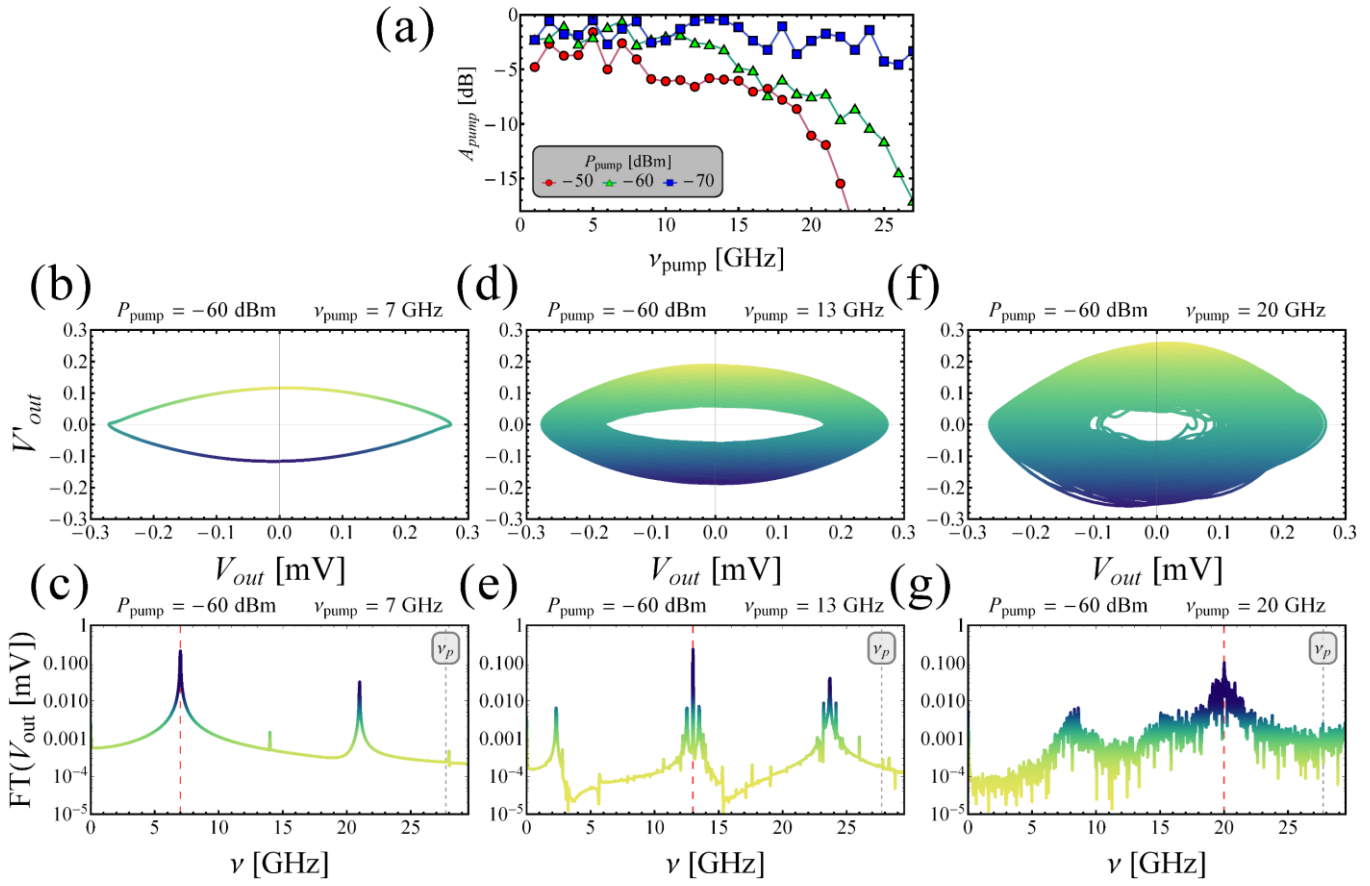
Fig. 3. Pump transmission regime. (a) Transmission loss, A_{pump}, as a function of the pump frequency, at different values of the pump power, in the absence of signal. (b-g) Phase-space portraits of $V_{out}(t)$, top panels, and the Fourier transforms (FTs), bottom panels, at different values of the pump frequency, ν_{pump}= 7 GHz, (b) and (c), 13 GHz, (d) and (e), and 20 GHz, (f) and (g), at a fixed pump intensity P_{pump}= -60 dBm. In the bottom panels, the vertical red and gray dashed line indicate the pump frequency and the plasma Josephson frequency ν_p, respectively.

nonlinearity of the system. In both cases, no current or magnetic biases are considered.

A.   Pump amplitude effects

We first excite the JTWPA with a pump tone with intensities $P_{pump} = [−70, −60, −50]$ dBm, which correspond to the voltage amplitudes $V_{pump} = [0.1, 0.32, 1]$ mV, respectively, in the absence of signal tone, $V_{sign} = 0$. The attenuation of propagating waves in the JTWPA is investigated calculating the quantity $A_{pump} = 20 \log [V_{out}(\nu_{pump})/V_{pump}]$, where $V_{out}(\nu)$ is the amplitude of the Fourier component of the output voltage, V_{out}, at a specific frequency.

In Fig. 3(a) we show the transmission loss, A_{pump}, as a function of the pump frequency ν_{pump}, at different values of the pump intensity. We first note that the higher ν_{pump}, the larger is the attenuation of the signal. However, the three curves shown in the figures *hide* quite different system behaviors. In fact, in the case of a low pump amplitude, $P_{pump} = −70$ dBm, the system response is always highly coherent, while on the contrary for large amplitudes values, $P_{pump} = −50$ dBm, the response is always incoherent and chaotic, and characterized by a larger attenuation. An intermediate situation occurs for $P_{pump} = −60$ dBm; in fact, in this case, increasing the pump frequency three

different regimes are encountered. To fully understand why and how this happens, we look at the dynamics of the output signal $V_{out}(t)$. Understanding the character of the dynamic response can be deepened through a frequency domain analysis. Note that the temporal dynamics and the Fourier analysis of the output voltage signal discussed in the following have been obtained neglecting an initial switch-on transient regime.

In the lower part of Fig. 3 we show the phase-space portraits (top panels) and the Fourier transforms (FTs) (bottom panels) of $V_{out}(t)$, obtained at three representative values of the pump frequency, $\nu_{pump} = 7$ GHz, (b-c), 13 GHz, (d-e), and 20 GHz, (f-g), keeping the pump intensity fixed at $P_{pump} = −60$ dBm. In the FT plots, the red and gray vertical dashed line indicates the pump frequency and the plasma Josephson frequency, respectively.

The response of the system is highly coherent and the time evolution periodic in the case of $\nu_{pump} = 7$ GHz; the phase-space portrait is characterized by a limit cycle, while the FT is formed by the main sharp peak at the pump frequency and smaller peaks at the higher-frequency overtones of the fundamental one, see Fig. 3(b-c). In this configuration the odd harmonics of the pump tone are much larger than the even ones, the reason being on evident. Instead, at a higher pump frequency, e.g., $\nu_{pump} = 13$ GHz in Fig. 3(d-e), the trajectory path enlarges
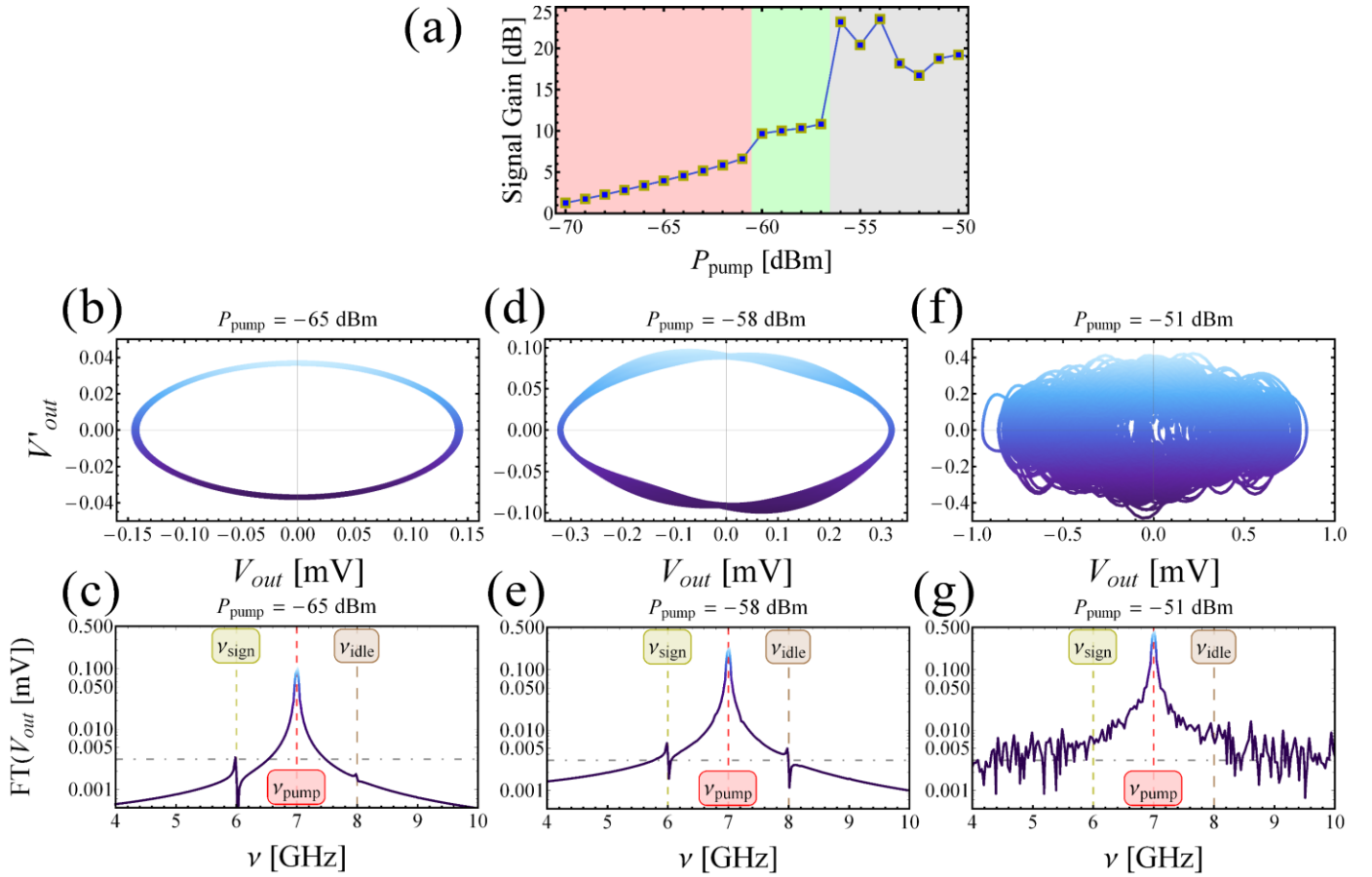
Fig. 4. Signal amplification regime. (a) Signal Gain, G_{sign}, as a function of the pump amplitude, at a fixed pump frequency $v_{pump} = 7$ GHz, and considering a small amplitude signal $P_{sign} = $ -100 dBm at a frequency $v_{sign} = 6$ GHz. Three different response regimes are highlighted by regions shaded in different colors. (b-g) Phase-space portraits of $V_{out}(t)$, top panels, and Fourier transforms (FTs), bottom panels, at different values of pump intensity, $P_{pump} = $ -65 dBm, (b) and (c), -58 dBm, (d) and (e), and -51 dBm, (f) and (g). These values fall each within one of the three shaded areas in panel (a). In the bottom panels, the vertical dashed lines indicate the frequencies of pump (red), signal (yellow), and idle (brown) tones, while the horizontal gray dot-dashed line marks the input signal intensity.

significantly, and the FT profile is composed by multipeaked structures, for it is enriched of additional peaks not merely commensurate. Finally, increasing further the pump frequency, e.g., $v_{pump} = 20$ GHz in Fig. 3(f-g), the system response becomes chaotic and the FT appears highly incoherent, with a noisy broad frequency spectrum. This regime is not suitable for application as an amplifier, as the pump power is distributed over the whole frequency spectrum.

B. Signal amplification

In the following, we discuss the case in which both a pump and a signal source are taken into account. In particular, we set the signal intensity at $P_{sign} = -100$ dBm, corresponding to a voltage amplitude $V_{sign} = 0.032$ mV, while the pump and signal frequencies are $v_{pump} = 7$ GHz and $v_{sign} = 6$ GHz, respectively. Thus, we expect an idle tone at $v_{idle} = 8$ GHz in the 4WM regime, since no bias is present.

In Fig. 4(a) we illustrate the behavior of the signal gain, G_{sign} = 20 log [$V_{out}(v_{sign})/V_{sign}$], as a function of the pump intensity P_{pump}. For the chosen parameters, the signal amplification is

systematically achieved for all the pump intensities considered in the figure. However, we note three different amplification regimes, evidenced by the colored zones in Fig. 4(a). For P_{pump} < -60 dBm (red-shaded region) a moderate gain is obtained, and G_{sign} increases linearly as P_{pump} increases up to $G_{sign} \leq 6$ dB. Then, for $P_{pump} \in [-60, -56]$ dBm the gain increases further up to values around $G_{sign} \sim 11$dB (green-shaded region). Finally, even larger pump amplitudes, i.e., $P_{pump} > -55$ dBm (gray-shaded region), seem to give quite larger gains, although, as we shall see below, this value does not correspond to a real amplification of the input signal.

It is useful also in this case to have a closed look at the time evolution of the output signal, in particular at the phase-space and FT of $V_{out}(t)$, Fig. 4(b-g). We set three different P_{pump} values to fit into each of the three different regimes described above. For a simpler reading of the Fourier spectra, we include vertical dashed lines to indicate the frequencies of pump (red), signal (yellow), and idle (brown) tones, while the horizontal gray dot-dashed line marks the input signal voltage amplitude V_{sign}.

We observe that for $P_{pump} = -65$ dBm, i.e., in the red-shaded region in Fig. 4(a), the phase-space portrait shows a curve approaching a sort of elliptical limit cycle, while the FT is

formed by clear peaks; in particular, we note the presence of a small peak at v_{sign} with a height slightly larger than V_{sign}, see Fig. 4(b-c).

The situation changes for P_{pump} values within the green-shaded region in Fig. 4(a). In this case, the phase-space shows a more complex limit cycle involving the three main frequencies, i.e., v_{pump}, v_{sign}, and v_{idle}, and the FT demonstrates clearly the signal tone amplification. In fact, at v_{sign} a Fourier peak stands out clearly above the input signal intensity, see Fig. 4(d-e) for $P_{pump} = -58$ dBm.

Finally, for a pump intensity within the gray shaded region in Fig. 4(a), the dynamics changes drastically, becoming chaotic. Indeed, the phase portrait consists of a closed, tangled skein, while the FT reveals a noisy background within which the weak-amplitude signal is completely hidden, see Fig. 4(f-g) for $P_{pump} = -51$ dBm.

IV. CONCLUSION

In this work, we have numerically explored the dynamics of a discrete array of rf-SQUIDs forming a JTWPA. The response to an input voltage formed either by one (a large pump tone) or two (a large pump and a small signal tone) components has been studied for different amplitudes and frequencies, corresponding to foreseen applications of JTWPA. The theoretical analysis faced the resolution of the system of $N=990$ coupled differential equations to describe each cell that constitutes the JTWPA, with the appropriate boundary conditions to account for the input and output signals; both the temporal dynamics and spectral analysis of the output were studied in detail. Assuming a realistic parameter setup, we have demonstrated the possibility to achieve a significant gain, up to $G_{sign} \sim 11$ dB (namely, a value incidentally very close to that observed in the early experiments by Zorin et al. [37]). Further optimizations of the values of the key parameters, as well as the use of different strategies, may realistically lead to even larger gains.

By numerical simulations of the JTWPA model equations, we have also demonstrated effects such as chaotic noise rise [38] and incommensurate frequency generation, that do not emerge in simplified lower-order approximation analytical approaches [20,23,26,27]. Our work allows the investigation of the effects of circuit parameters on the performances of a JTWPA. Moreover, within this approach the effect of fluctuations, due to the fabrication or operation process, of the discrete array parameters can also be addressed.

Finally, we observe that the emergence of chaotic effects in Josephson arrays is a well-known phenomenon, and strategies have been proposed to avoid it. For example, proper spacing between chains should be chosen to suppress the possible jitter accumulation [39] that can also transfer to chaotic dynamics, and an efficient load matching can suppress a chaotic regime [40]. Furthermore, taking thermal fluctuations into account, the joint effect of chaos and noise can lead to a further increase in the overall noise level [40]. In this regard, the effect of noise has to be considered when studying the behavior of Josephson systems and the RCSJ model [8,41]. In particular, Josephson junctions are ideal candidates for characterizing the statistics of noise affecting the system, also in the light of unveiling the

properties of an unknown noise source embedded in a thermal noise background [41,42,43].

V. REFERENCES

[1] B. Xiong, et al., "Improve microwave quantum illumination via optical parametric amplifier," Annals of Physics, vol. 385, pp. 757–768, 2017, ISSN: 0003-4916. doi: 10.1016/j.aop.2017.08.024

[2] L. Fasolo, et al., "Josephson Traveling Wave Parametric Amplifiers as non-classical light source for Microwave Quantum Illumination", Measurement: Sensors, vol. 18, p. 100349, 2021, https://doi.org/10.1016/j.measen.2021.100349.

[3] S. J. Weber, et al., "Mapping the optimal route between two quantum states," Nature, vol. 511, no. 7511, pp. 570–573, 2014, ISSN: 1476-4687. doi: 10.1038/nature13559.

[4] Z. R. Lin, et al., "Single-shot readout of a superconducting flux qubit with a flux-driven josephson parametric amplifier," Applied Physics Letters, vol. 103, no. 13, p. 132 602, 2013., doi: 10.1063/1.4821822.

[5] Y. F. Chen, et al., "Microwave photon counter based on Josephson junctions", Phys. Rev. Lett., vol. 107, p 217401, 2011, doi: 10.1103/PhysRevLett.107.217401.

[6] C. Guarcello, et al., "Josephson-Threshold Calorimeter", Phys. Rev. Appl., vol. 11, n. 054074, 2019, doi:10.1103/physrevapplied.11.054074

[7] L. S. Revin, et al. "Microwave photon detection by an Al Josephson junction", Beilstein J. Nanotechnol., vol. 11, n. 960, 2020, doi:10.3762/bjnano.11.80

[8] C. Guarcello, et al., "Josephson-based scheme for the detection of microwave photons", Phys. Rev. Appl., vol. 16, n. 054015 2021, doi: 10.1103/PhysRevApplied.16.054015

[9] A. Piedjou Komnang, et al., "Analysis of Josephson junctions switching time distributions for the detection of single microwave photons", Chaos Solitons Fractals, vol. 142, p. 110496, 2021, doi: 10.1109/WOLTE49037.2021.9555447.

[10] A. L. Pankratov., et al., "Approaching microwave photon sensitivity with Al Josephson junctions", Beilstein J. Nanotechnol., vol. 13(1), 582, 2022, doi: 10.3762/bjnano.13.50

[11] L. Fasolo et al., "Bimodal Approach for Noise Figures of Merit Evaluation in Quantum-Limited Josephson Traveling Wave Parametric Amplifiers," in IEEE Transactions on Applied Superconductivity, vol. 32, no. 4, pp. 1-6, June 2022, Art no. 1700306, doi: 10.1109/TASC.2022.3148692.

[12] J. Aumentado, "Superconducting Parametric Amplifiers: The State of the Art in Josephson Parametric Amplifiers," IEEE Microw. Mag., vol. 21, no. 8, pp. 45–59, Aug. 2020, doi: 10.1109/MMM.2020.2993476.

[13] F. Lecocq et al., "Nonreciprocal Microwave Signal Processing with a Field-Programmable Josephson Amplifier," Phys. Rev. Appl., vol. 7, no. 2, Feb. 2017, Art. no. 024028, doi: 10.1103/PhysRevApplied.7.024028.

[14] P. Krantz et al.," A quantum engineer's guide to superconducting qubits," Appl. Phys. Rev., vol. 6, no. 2, May 2019, Art. no. 021318; doi: 10.1063/1.5089550.

[15] I. Siddiqi, Engineering high-coherence superconducting qubits. Nat Rev Mater. Vol 6, pp. 875–891, 2021, https://doi.org/10.1038/s41578-021-00370-4

[16] S. Al Kenany et al., "Design and operational experience of a microwave cavity axion detector for the 20-100 μeV range," Nucl. Instrum. and Meth. in Phys. Res. A, vol. 854, pp. 11-24, May 2017, doi: 10.1016/j.nima.2017.02.012.

[17] A. L. Pankratov, A. et al. "Towards a microwave single-photon counter for searching axions", npj Quantum Inf., vol.8, n.61, 2022, doi:10.1038/s41534-022-00569-5

[18] R. Grimaudo, et al., "Josephson-junction-based axion detection through resonant activation", Phys. Rev. D, vol. 105, n. 033007, 2022, doi:10.1103/physrevd.105.033007

[19] A.L. Cullen, "Theory of the travelling-wave parametric amplifier," Proc. of IEE - Part B: Electron. and Commun. Eng, vol. 107, no. 32, pp. 101-107, May 1960, doi: 10.1049/pi-b-2.1960.0085.

[20] M. Sweeny and R. Mahler, "A travelling-wave parametric amplifier utilizing Josephson junctions," IEEE Trans. on Magn., vol. 21, no. 2, pp. 654-655, March 1985, doi: 10.1109/TMAG.1985.1063777.

[21] C. Macklin et al., "A near–quantum-limited Josephson traveling-wave parametric amplifier", Science, vol. 350, no. 6258, pp. 307-310, Oct. 2015, doi: 10.1126/science.aaa8525.

[22] M. T. Bell and A. Samolov, "Traveling-Wave Parametric Amplifier Based on a Chain of Coupled Asymmetric SQUIDs," *Phys. Rev. Appl.*, vol. 4, no. 2, Aug. 2015, Art. no. 024014, doi: 10.1103/PhysRevApplied.4.024014.

[23] A. B. Zorin, "Josephson Traveling-Wave Parametric Amplifier with Three-Wave Mixing," *Phys. Rev. Appl.*, vol. 6, no. 3, Sep. 2016, Art. no. 034006, doi: 10.1103/PhysRevApplied.14.034058.

[24] N. E. Frattini *et al*, "Optimizing the Nonlinearity and Dissipation of a SNAIL Parametric Amplifier for Dynamic Range," *Phys. Rev. Appl.*, vol. 10, no. 5, Nov. 2018, Art. no. 054020, doi: 10.1103/PhysRevApplied.10.054020.

[25] A. B. Zorin, "Flux-Driven Josephson Traveling-Wave Parametric Amplifier," *Phys. Rev. Appl.*, vol. 12, no. 4, Oct. 2019, Art. no. 044051, doi: 10.1103/PhysRevApplied.12.044051.

[26] T. Dixon *et al*, "Capturing Complex Behavior in Josephson Traveling-Wave Parametric Amplifiers," *Phys. Rev. Appl.*, vol. 14, no. 3, Sep. 2020, Art. no. 034058, doi: 10.1103/PhysRevApplied.6.034006.

[27] L. Planat *et al.*, "Photonic-Crystal Josephson Traveling-Wave Parametric Amplifier," *Phys. Rev. X*, vol. 10, no. 2, Apr. 2020, Art. no. 021021, doi: 10.1103/PhysRevX.10.021021.

[28] A. Greco, *et al*., "Quantum model for rf-SQUID-based metamaterials enabling three-wave mixing and four-wave mixing traveling-wave parametric amplification", *Phys. Rev. B* vol. 104, n 184517, 2021, doi: 10.1103/PhysRevApplied.14.034058.

[29] L. Fasolo, A. Greco and E. Enrico, "Superconducting Josephson-Based Metamaterials for Quantum-Limited Parametric Amplification: A Review," in Advances in Condensed-Matter and Materials Physics - Rudimentary Research to Topical Technology, J. Thirumalai and S. I. Pokutnyi Ed., IntechOpen, Rijeka, Croatia, 2020, doi: 10.5772/intechopen.89305.

[30] M. Esposito *et al*, "Perspective on traveling wave microwave parametric amplifiers," *Appl. Phys. Lett*., vol. 119, n. 120501, 2021, doi:10.1063/5.0064892

[31] A. Giachero "Detector Array Readout with Traveling Wave AmplifieRS", J Low Temp Phys (2022), doi:10.1007/s10909-022-02809-6

[32] S. Pagano *et al.*, "Development of Quantum Limited Superconducting Amplifiers for Advanced Detection," in *IEEE Transactions on Applied Superconductivity*, vol. 32, no. 4, pp. 1-5, June 2022, Art no. 1500405, doi: 10.1109/TASC.2022.3145782.

[33] A. Barone, G. Paternò, Physics and Applications of the Josephson Effect; Wiley: New York, NY, USA, 1982.

[34] O. Yaakobi *et al.*, "Parametric amplification in Josephson junction embedded transmission lines," *Phys. Rev. B*, vol. 87, no. 14, Apr. 2013, Art. no 144301, doi: 10.1103/PhysRevB.87.144301.

[35] K. O'Brien *et al.*, "Resonant Phase Matching of Josephson Junction Traveling Wave Parametric Amplifiers," *Phys. Rev. Lett.*, vol. 113, no. 15, Oct. 2014, Art. no. 157001, doi: 10.1103/PhysRevLett.113.157001.

[36] S. Ó. Peatáin, "The Effect of Parameter Variations on the Performance of the Josephson Travelling Wave Parametric Amplifiers", 2021. [Online]. Available: https://arxiv.org/abs/ 2112.07766

[37] A. B. Zorin, *et al*., "*Traveling-Wave Parametric Amplifier Based on Three-Wave Mixing in a Josephson Metamaterial*," 2017 16th International Superconductive Electronics Conference (ISEC), 2017, pp. 1-3, doi: 10.1109/ISEC.2017.8314196.

[38] M. Esposito, *et al*. "Observation of Two-Mode Squeezing in a Traveling Wave Parametric Amplifier", *Phys. Rev. Lett*. vol 128, p. 153603, 2022, doi:10.1103/PhysRevLett.128.153603

[39] I. I. Soloviev, *et al.*, "Effect of Cherenkov radiation on the jitter of solitons in the driven underdamped Frenkel-Kontorova model", *Phys. Rev. E* vol. 87, p. 060901, 2013, https://doi.org/10.1103/PhysRevE.87.060901

[40] A. L. Pankratov, *et al*., "Oscillations in Josephson transmission line stimulated by load in the presence of noise", *Appl. Phys. Lett.* vol. 110, p. 112601, 2017, https://doi.org/10.1063/1.4978514

[41] C. Guarcello and F. Bergeret, "Cryogenic Memory Element Based on an Anomalous Josephson Junction", *Phys. Rev. Applied* vol. 13, p. 034012, 2020, https://doi.org/10.1103/PhysRevApplied.13.034012

[42] C. Guarcello, *et al*., "Josephson-based Threshold Detector for Lévy-Distributed Current Fluctuations", *Phys. Rev. Applied* vol. 11, p. 044078, 2019, https://doi.org/10.1103/PhysRevApplied.11.044078

[43] C. Guarcello, *et al*., "Voltage drop across Josephson junctions for Lévy noise detection" *Phys. Rev. Research* vol. 2, p. 043332, 2020, https://doi.org/10.1103/PhysRevResearch.2.043332

[44] C. Guarcello, "Lévy noise effects on Josephson junctions", *Chaos, Solitons Fractals*, vol. 153, p. 111531, 2021, https://doi.org/10.1016/j.chaos.2021.111531